p emission rates in K absorptions at rest on Li6, Li7, Be9, C13, and O16

$\Sigma^- p$ emission rates in K^- absorptions at rest on ^{6}Li, ^{7}Li, ^{9}Be, ^{13}C, and ^{16}O

M. Agnello,[8,11] L. Benussi,[4] M. Bertani,[4] G. Bonomi,[3,6] E. Botta,[9,11] M. Bregant,[13,*] T. Bressani,[9,11] S. Bufalino,[11] L. Busso,[9,11] D. Calvo,[11] P. Camerini,[12,13] B. Dalena,[1,2,†] F. De Mori,[9,11] G. D'Erasmo,[1,2] A. Feliciello,[11] A. Filippi,[11,‡] E. M. Fiore,[1,2] A. Fontana,[6] H. Fujioka,[5] P. Genova,[6] P. Gianotti,[4] N. Grion,[13] V. Lucherini,[4] S. Marcello,[9,11] O. Morra,[10,11] T. Nagae,[5] H. Outa,[7] A. Pantaleo,[2,§] V. Paticchio,[2] S. Piano,[13] R. Rui,[12,13] G. Simonetti,[2] R. Wheadon,[11] and A. Zenoni[3,6]
(FINUDA Collaboration)
[1]*Dipartimento di Fisica, Università di Bari, 70125 Bari, Italy*
[2]*I.N.F.N. Sezione di Bari, 70125 Bari, Italy*
[3]*Dipartimento di Ingegneria Meccanica e Industriale, 25123 Brescia, Italy*
[4]*I.N.F.N. Laboratori Nazionali di Frascati, 00044 Frascati, Italy*
[5]*Department of Physics, Kyoto University, Kitashirakawa, Kyoto 606-8502, Japan*
[6]*I.N.F.N. Sezione di Pavia, 27100 Pavia, Italy*
[7]*RIKEN, Wako, Saitama 351-0198, Japan*
[8]*Dipartimento di Fisica, Politecnico di Torino, 10129 Torino, Italy*
[9]*Dipartimento di Fisica, Università di Torino, 10125 Torino, Italy*
[10]*I.N.A.F.-I.F.S.I., Sezione di Torino, 10133 Torino, Italy*
[11]*I.N.F.N. Sezione di Torino, 10125 Torino, Italy*
[12]*Dipartimento di Fisica, Università di Trieste, 34127 Trieste, Italy*
[13]*I.N.F.N. Sezione di Trieste, 34127 Trieste, Italy*
(Received 14 August 2015; published 21 October 2015)

An experimental study of the $K^-_{\rm stop}A \to \Sigma^- pA'$ reaction on $A = {}^6$Li, ^{7}Li, ^{9}Be, ^{13}C, and ^{16}O p-shell nuclei is presented. The data were collected by the FINUDA spectrometer operating at the DAΦNE ϕ factory (LNF-INFN, Italy). Emission rates for the reaction in the mentioned nuclei are measured and compared with the few existing data. The spectra of several observables are discussed; indications of quasifree absorptions by a (np) pair embedded in the A nucleus can be obtained from the study of the missing mass distributions.

DOI: 10.1103/PhysRevC.92.045204 PACS number(s): 21.45.−v, 21.80.+a, 25.80.Nv

I. INTRODUCTION

The existing measurements of kaon absorption reactions by two or few nucleons are scarce and, for the largest part, dated. Only one paper describes in good detail the interaction of K^-'s at rest on ^{4}He in a bubble chamber [1]. More recently, data have been collected on ^{4}He by the E549 experiment at KEK [2]. Just few other data, with large or even no quoted errors, exist. They were taken in emulsion experiments, which studied the interaction of K^-'s with nuclei heavier than ^{16}O [3], or in bubble chambers filled with hydrocarbon mixtures or neon [4].

The existing measurements suggest a surface behavior of the kaonic absorption; they indicate that the contribution of kaonic absorption reactions containing at least one nucleon in the final state is as sizable as ∼20%, in medium-heavy nuclei [1,4]. Given such a high rate, a more detailed knowledge on the absorption features is desirable; in fact, these processes represent the main background under the signals of hypernuclei formation in kaon induced reactions [5]. Hypernuclear capture rates are, in comparison, at least one order of magnitude smaller. Therefore, reliable studies of hypernuclei formed by kaons interacting at rest with rates of the order of $10^{-4} - 10^{-5}/K^-_{\rm stop}$, or of decays of hypernuclei in rare modes [6], need a precise definition of such background reactions.

More detailed information on the rates of kaon induced reactions in nuclei is also relevant for astrophysical investigations, for instance concerning the composition of possible compact stars with hyperonic content, an issue related to the so-called "hyperon puzzle" [7]. The presence of hyperons in dense nuclear matter could have sizable effects on the softness of the compact star equation of state (EOS); moreover, their many-body interactions with nucleons could have a direct impact on the possible maximum value of the star mass. The models based on standard nuclear physics approaches rely heavily on the still approximate knowledge of the interactions between hyperon(s) and nucleon(s), that can be derived only from the few existing experimental data on hyperon-nucleon scattering or from reactions involving hypernuclei. New and precise experimental inputs are therefore awaited to provide reliable constraints on several parameters of the models, still loosely defined. This will open the possibility to improve the description of dense stellar objects able to reproduce the most recent astrophysical measurements of their mass.

In addition, the processes of K^- absorption by two or few nucleons could be at the basis of the possible formation of kaon-nuclear bound states, assumed to be aggregates of

*Present address: Universidade de São Paulo, 05508-070 São Paulo, Brazil.
†Present address: CEA/SACLAY, DSM/Irfu/SACM, 91191 Gif-sur-Yvette, France.
‡Corresponding author: filippi@to.infn.it.
§Deceased.

nucleons strongly bound by an antikaon. The existence of such states was predicted some years ago [8] and over the last years several experiments have been pursuing their search. Some observations were reported for a bound $K^- pp$ system decaying in Λp [9–13], but they are still awaiting confirmation. Even if its observability could be questioned as a consequence of the theoretically expected large widths [14], its existence is not ruled out yet, as well as those of different isospin partners that could be observed, for instance, in K^- absorptions producing ΣN pairs.

This paper presents a study of the $K^-_{\rm stop} A \to \Sigma^- p A'$ reaction on ^{6}Li, ^{7}Li, ^{9}Be, ^{13}C, and ^{16}O, which enriches the existing meager set of available data. The data were collected in 2006–2007 by the FINUDA experiment, a magnetic spectrometer installed at the e^+e^- DAΦNE collider, Laboratori Nazionali dell'INFN di Frascati (LNF), Italy.

This study follows a first analysis of kaon absorption by one nucleon producing $\Sigma^\pm\pi^\mp$ final states [15], on the mentioned nuclear species. In the present analysis final states with one neutron, one negative pion, and one proton only are selected. The π^- and the neutron can come from the Σ^- hyperon decay $\Sigma^- \to n\pi^-$, branching ratio (B.R.) = 99.85%; the proton can be emitted promptly in the elementary $K^-_{\rm stop}(np) \to \Sigma^- p$ two-nucleon absorption on a quasideuteron embedded in the A nucleus. Hyperon (Y) and nucleon (N) pairs can also be emitted inclusively, together with other particles, in many-nucleon absorptions. The absorption mechanism is expected to follow the "quasifree" (QF) pattern [16]: the kaon interacts at rest with a nucleon pair (or cluster) having a Fermi momentum typical of the target nucleus [17] and a YN pair is subsequently emitted; the spectator nucleus recoils with opposite momentum, in the nucleus center of mass. Since the kaons interact at rest and close to the nuclear surface [1], it is unlikely for the K^- to be absorbed by the whole nucleus with a following isotropic phase space emission of Σ^-, p, and A' [16], so this possibility has been discarded throughout this work.

An earlier semi-inclusive analysis was performed by FINUDA on a first set of data, in which the π^- and the proton only were detected [18]. The $\Sigma^- p$ emission rate for K^- induced interaction on ^{6}Li was assessed, with evidence that the signal observed in the proton momentum distribution was a signature of a two-nucleon QF absorption on ^{6}Li. A less clean signature was obtained in a nucleus as heavy as ^{12}C, due to a stronger dilution effect caused by final state interactions (FSI in the following). The experimental signature of a two-nucleon QF kaon absorption is given by a hyperon-nucleon pair emitted both with a momentum typically larger than 400 MeV/c. The particles from the Σ^- decay have a continuous momentum distribution that in FINUDA, for negative pions, extends from ∼80 to ∼350 MeV/c, and overlaps thus completely the momentum region of π^-'s from hypernuclear formation.

This paper is organized as follows. In Sec. II a short account of the experimental setup, already fully sketched out elsewhere [19], is given; in Sec. III the data selection criteria are described. In Sec. IV a study of the features of some experimental spectra is presented. ^{6}Li is chosen as reference nucleus, due to its relatively simple structure and the cleanest signatures it can provide. ^{6}Li, as known from pion absorption experiments [20], can in fact be understood as formed by a "quasi"-α nucleus together with a $p+n$ pair or a loosely bound "quasideuteron". The Fermi momentum of the ^{6}Li subclusters can be modeled with fair accuracy [21], so precise studies of quasifree absorptions are possible. In addition, with a nucleus as light as ^{6}Li the effects of FSI of the emitted particles with the residual nucleus are limited.

The study of the distribution of the missing mass between the initial state and the measured particles shows that some contributions of different QF reactions producing $\Sigma^- p$ pairs, alone or together with other undetected particles, can be distinguished. Emission rates of QF $\Sigma^- p$ reactions can be evaluated, per $K^-_{\rm stop}$, for the mentioned p-shell nuclei. The followed procedure is described in Sec. V. For the sake of conciseness, throughout the paper we will indicate as "semi-inclusive" the emission of $\Sigma^- p$ pairs recoiling against a nuclear system in its minimal mass configuration (coinciding with the ground state for stable nuclei, within the experimental resolution), while the notation "inclusive" will refer to the generic $A(K^-_{\rm stop}, \Sigma^- pX)A'$ reaction, where X can be any particle escaping detection, and A' the recoiling nucleus in whichever energetic configuration. Capture rates are evaluated for both cases.

The obtained results are reported in Sec. V, while the discussion of the results with a comparison with the few existing data and the conclusions follow in Sec. VI.

II. EXPERIMENTAL SETUP

The DAΦNE e^+e^- collider at LNF provides $\phi(1020)$ mesons with a luminosity of some 10^{32} cm^{-2} s^{-1}. The $\phi(1020)$, produced almost at rest, decays about half of the times into a pair of slow (16.1 ± 1.5 MeV), almost back-to-back charged kaons. A slight asymmetry in the $\phi(1020)$ decay is due to a small crossing angle between the colliding beams, which gives the $\phi(1020)$ a small boost.

FINUDA studied the reactions induced by the charged kaons. In particular, the K^- could be stopped in a set of eight thin targets (∼0.25 g/cm^2), arranged coaxially as tiles around the beam and composed of materials of pure isotopic composition with a mass number chosen in the range $6 \leqslant A \leqslant 51$. In the years 2003–2007, in two runs, data corresponding to about 1.2 fb^{-1} of (e^+e^-) collisions at the ϕ energy were collected. The apparatus consisted of a magnetic spectrometer with cylindrical symmetry, of 125 cm radius and 255 cm maximum length, immersed in a 1-T solenoidal magnetic field provided by a superconducting magnet and uniform to better than a few percent.

The apparatus was able to detect the kaons before they reached the targets by means of a thin scintillator hodoscope surrounding the beam pipe (named TOFINO in short) [22], and an inner vertex detector composed of one layer of eight double-sided silicon microstrip modules (named ISIM) [23]. A dedicated algorithm, with a maximum inefficiency of ∼2% (modulated depending on the target position), was developed to correctly identify the charge and momentum of the kaon before impinging on the target; it exploited the available geometric and kinematic information. Beyond the target array, the tracking of the charged particles emitted in

the negative kaon interactions was performed; a momentum resolution as good as 0.6% full width at half maximum (FWHM) was achieved. The tracking detectors stack consisted of one layer of ten double-sided silicon microstrip modules (called OSIM) [23], two layers of eight planar low-mass drift chambers (LMDCs) at a distance, respectively, of about 37 and 65 cm from the beam axis [24], and a six-layer array of stereo-staggered straw tubes [25]. The tracking detectors were held by an aluminum clepsydra-shaped frame. The whole tracking region was filled and fluxed with helium gas to minimize multiple scattering of the emitted particles. The silicon detectors and the drift chambers allowed also for the particle identification by means of the energy lost in their active volume. Along with the time-of-flight (TOF) information, light minimum ionizing particles could be separated from protons with an identification efficiency as large as 98%. Deuterons and tritons could also be observed and identified, respectively, above 300 [26] and 430 MeV/c [27]. The TOF information was provided by a system composed of the TOFINO scintillator array as start detector, and a stop scintillator barrel, 10 cm thick, located outside the tracking region and facing the magnet coil (named TOFONE) [28]. The system delivered the trigger signal to the detector, and TOFONE also allowed the detection of neutrons with an efficiency of about 10%.

III. DATA SELECTION

The analysis presented in this paper is performed on the data collected in the second of the two FINUDA data takings (966 pb^{-1}). In this run p-shell nuclei targets were used (solid: 2 $\times^6$ Li, 2 $\times^7$ Li, 2 $\times^9$ Be; powder: ^{13}C; liquid: ^{16}O, in the form of deuterated water contained in an aluminum-polycarbonate film envelope). The trigger thresholds set in the first data taking did not allow neutrons with energy below 11 MeV to be detected [29]; therefore these data cannot be effectively used in the present analysis, as too few useful Σ^-'s would be available after reconstruction.

($n\pi^- p$) events are selected requiring the proton and the incoming K^- to form the same vertex. The spatial resolution of the K^- stop point coordinates is 700 μm, evaluated through an extrapolation of the incoming track to the target by means of the GEANE package [30]. A cut on the distance of minimum approach of the π^- and the vertex in the target is applied tailored to the target thickness and its spatial location, to allow the reconstruction of a Σ^- secondary decay vertex. The minimum distance is required to be 1 to 1.2 cm. High quality tracks (χ^2 out of the track fitting procedure corresponding to a probability of correctly reconstructing a track larger than 95%) are selected for both π^- and proton. Tracks hitting the aluminum frame supports and not long enough to reach at least the first drift chamber layer are discarded.

The momentum resolution of charged particles is not crucial for this analysis. As reference, for π^+'s of 184.5 MeV/c from the Σ^+ decay at rest the FINUDA momentum resolution was 1% [15]; it worsened for lower momenta due to the smaller number of points available for tracking, while it improved up to 0.6% for momenta of about 240 MeV/c, as measured from $K_{\mu 2}$ decays [19]. From the same Σ^+ decay, the momentum resolution of neutrons was assessed to be 5% [15]. We recall that the detection of neutrons is performed by means of a time of flight measurement on a base of flight of 2 m at most.

Neutrons in FINUDA are heavily contaminated by the huge background of γ's from various particles' decays. In addition, some of them are subject to rescattering before being detected by TOFONE. The cut on the neutron speed applied in the analyses of Refs. [15,31] is partially released ($1/\beta > 1$), to increase the neutron acceptance at all momenta. However, in this way a large number of γ's and fake neutrons leaks in the sample. Neutrons are identified when isolated TOFONE slabs (or pairs thereof) are found not connectable to any charged track in the spectrometer, or far from spurious signals in the straw array that could derive from particles backscattered by the magnet yoke. An upper cut to $1/\beta$ ($<$12) is applied to reduce this effect. In the case of multiple neutron candidates per event, their identification quality follows their energy deposit on TOFONE slabs. In the present analysis, events are accepted if one neutron only is identified.

The background from fake neutral particles and from other contaminating QF reactions which can stem from the same final state can be effectively reduced only after the application of proper kinematic cuts to the data. In fact, the reconstruction efficiency for all neutral particles identified in FINUDA by TOF is barely similar (averaged over the eight targets: $(3.50 \pm 0.01) \times 10^{-2}$ for neutrons, $(2.16 \pm 0.01) \times 10^{-2}$ for γ's, $(2.33 \pm 0.01) \times 10^{-2}$ for π^0's); therefore, the possibility to discard contaminations from neutral particles other than neutrons mainly relies on a kinematic identification of the searched reaction.

The main physical contribution to the ($n\pi^- p$) sample is given by the Λn final state, produced through a direct QF two-body absorption at the level of a few percent [1], or via a Σ-Λ conversion reaction, in both cases with the Λ decaying in ($\pi^- p$) pairs (B.R. = 64%). In the present analysis Λ's in the final state are eliminated by means of a cut on the invariant mass of the detected ($\pi^- p$) pair and on their angular correlation; in fact, the Λ in this QF reaction is produced with high momentum, thus the particles from its decay are mostly forward emitted. To this purpose, events are rejected if with $\cos\theta_{p\pi^-} > 0.6$. The loss of Σ^- events due to the application of these cuts is negligible.

A second large contamination comes from the QF one-nucleon $K^- p \to \Sigma^+ \pi^-$ reaction, followed by either $\Sigma^+ \to p\pi^0$ with one of the γ's from π^0 mimicking a neutron (or by $\Sigma^+ \to n\pi^+$ with a π^+/p misidentification, whose occurrence is however thoroughly suppressed thanks to the apparatus particle identification capabilities), or by a $\Sigma^+ n \to \Lambda p$ conversion and the following $\Lambda \to n\pi^0$ decay (B.R. = 36%). In the latter case, a π^0 is missing. The $\Sigma^+\pi^-$ QF absorption on one nucleon occurs with an emission rate of about 18%/$K^-_{\rm stop}$ in ^{6}Li [15], so the contamination of this channel can be quite sizable. The largest part of these events can be rejected applying a cut on the secondary vertex distance and, eventually, on the missing mass of the reaction. This quantity, defined as

$$\mathcal{M} = \sqrt{(M_A - E_n - E_{\pi^-} - E_p)^2 - (\vec{p}_n + \vec{p}_{\pi^-} + \vec{p}_p)^2}, \quad (1)$$

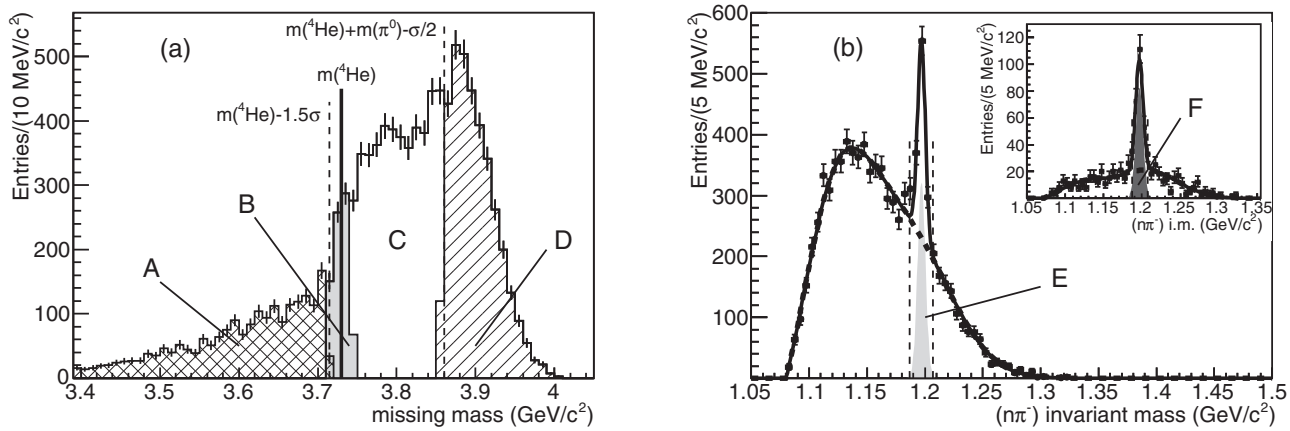

FIG. 1. (a) Missing mass of the $K^-_{\rm stop}$ ^{6}Li $\rightarrow n\pi^- pA'$ reaction: the vertical lines mark the ^{4}He mass value (solid), and the lower limits set for the $K^-_{\rm stop}$ ^{6}Li $\rightarrow (\Sigma^- p)^4$He and $K^-_{\rm stop}$ ^{6}Li $\rightarrow (\Sigma^- p\pi^0)^4$He (dashed) reaction selection. The cross-hatched area (A) is filled by unphysical events, the grey one (B) by events from the QF $K^-_{\rm stop}$ ^{6}Li $\rightarrow (n\pi^- p)^4$He reaction, the hatched one (D) by events compatible with the presence of at least one undetected π^0. (b) Invariant mass of the $(n\pi^-)$ system for the $K^-_{\rm stop}$ ^{6}Li $\rightarrow n\pi^- pA'$ reaction: in the inset events selected in the grey area (B) of (a) are selected. The grey-filled Gaussian areas correspond to the Σ^- signals; see text for details. The regions denoted as E and F and delimited by dashed vertical lines indicate, in the two plots, the chosen mass window for the evaluation of the Σ^- signal integral.

where M_A is the mass of the target nucleus, and E and $\vec{p}$ are the energy and momentum vector of the three measured particles, is shown in Fig. 1(a) for the ^{6}Li$(K^-_{\rm stop},n\pi^- p)A'$ reaction, after the cuts for the mentioned contaminations. ^{6}Li is shown as a typical case; spectra from other targets are similar. For ease of observation, the spectra in Fig. 1 are not corrected by the apparatus acceptance, which will be accounted for in the following.

A large part of events in the missing mass distribution, to the left of the mass value of the ground state of the recoiling nucleus (in the case of ^{6}Li: ^{4}He mass, 3.73 GeV/c^2), are affected by a wrong neutron momentum evaluation or misidentification. They mainly derive from the mentioned γ-neutron misidentification and from neutrons scattered before detection, to which a larger momentum is incorrectly assigned. A large source of photons is the mentioned single nucleon absorption in $\Sigma^+\pi^-$, with $\Sigma^+ \rightarrow p\pi^0$ (B.R. = 51.57%); as well, all QF reactions involving Σ^0's produce γ's. Also a small number of physical $\Sigma^- p$ events (less than 10% of the total semi-inclusive sample) belong to this region, those in which more than one nucleon is emitted in the absorption. Since events with one neutron only are accepted, a misidentification between the prompt and the Σ^- decay neutron may have occurred in this case.

For the sake of brevity the recoiling configuration with minimum mass will be denoted in the following as $A'_{g.s.}$, as a shortcut valid also for the cases in which the recoiling system is unstable (like, e.g., ^{5}He). Due to the missing mass resolution, which varies in the range 9–13 MeV/c^2 according to the target location and composition, the notation $A'_{g.s.}$ thus includes also fragmented recoiling nuclear systems, produced in the absorption on three nucleons or more, which cannot be distinguished from the ground state.

In Fig. 1(a) the vertical solid line marks the $A' \equiv {}^4$He mass, and the dashed one on the left the lower limit chosen for the analysis. The events in the cross-hatched area, indicated in the plot as A, are removed from the studied sample. Monte Carlo evaluations show that this cut rejects just a negligible number of physical $\Sigma^- p$ events.

The $(n\pi^-)$ invariant mass of the remaining events for the ^{6}Li target is displayed in Fig. 1(b). The central value of the Σ^- signal is at $[1197.0 \pm 3.4(\sigma)]$ MeV/c^2, from a fit by means of a Gaussian function superimposed to a fifth order Chebychev polynomial. The integral of the peak within $\pm 2\sigma$ and of the polynomial background (B) in the same mass interval [the region marked as E in Fig. 1(b)] gives the signal (S) sensitivity $\mathscr{S} = S/\sqrt{S+B} = 15.48$, corresponding to a signal/background ratio $S/B = 0.84$.

In the missing mass distribution displayed in Fig. 1(a) at least two parts may be singled out which can be addressed as signatures of distinct QF two-nucleon K^- absorptions. Around the ^{4}He mass value, a small enhancement, two bins wide, can be observed: it is due to the K^- ^{6}Li $\rightarrow \Sigma^- p^4$He two-body QF reaction (grey solid area in the plot, labeled as B), plus many-nucleon absorptions in which the four-nucleon recoiling system mass falls within the missing mass selected range. The extension of the grey area, corresponding to three times the missing mass experimental resolution, is chosen to minimize the contributions of these many-nucleon absorptions. Depending on the target nucleus, the suppression of the overlapping reactions is, though, only partly successful. A 3σ range allows us to discard the completely fragmented recoiling configurations, for all the studied nuclei. Conversely, configurations in which one or two more nucleons are emitted together with the remainder of the nuclear system can be separated from the minimal mass configuration with an efficiency that is usually larger for heavier nuclei. Since the relative occurrence of each of these reactions is unknown, in the following an integrated rate only will be quoted.

A second enhancement can be seen at higher missing mass where the threshold for π production opens: the hatched grey area in the plot (D) corresponds to events compatible with the K^- ^{6}Li $\rightarrow \Sigma^- p\pi^0$ A' QF reaction, in which the π^0 escapes detection.

These two classes of reactions alone cannot explain the central bulk of the spectrum, indicated in the figure as C (open area). This area may be filled by contaminating background reactions which feed the $(np\pi^-)$ final state as well as by QF $\Sigma^- p$ two nucleon absorptions (recoiling against nuclear systems in different energy configurations) possibly followed by FSI of the emitted particles, or by many-nucleon absorptions with the emission of Σ^-, p, and additional, undetected, nucleons and pions.

A quantitative study of the most likely contaminating reactions leaking through the data selection criteria has been performed by means of Monte Carlo simulations. Table I reports the values of these contaminations per generated event, averaged over the eight available targets: the simulated events are filtered through the reconstruction and analysis chain and selected in the Σ^- invariant mass band (E region).

According to the position of the target, different sectors of the spectrometer are spanned by the tracks, with different detector efficiencies; the error quoted in Table I is systematic and takes into account their maximum spread. The statistical error, in comparison, is negligible.

The main contaminating contribution, on the order of 10^{-5}/event, is given by the one-nucleon $K^- p \to \Sigma^+ \pi^-$ absorption; the contamination of the other reactions to the selected sample is at least one order of magnitude less. For the sake of comparison, the reconstruction efficiency for the $K^-_{\rm stop}(np)\ [A-np] \to \Sigma^- p\ [A-np]$ QF reaction is reported in the last line of the table.

The experimental spectra displayed in the following are corrected for the apparatus acceptance. The acceptance correction is made per event and is determined through the generation of about $3 \times 10^9 K^-_{\rm stop} A \to n\pi^- p A'$ events with uniform distribution of the final particle momenta over a wide kinematic range, exceeding that allowed by the QF reactions under study. The acceptance function is determined in each cell of the multidimensional array containing the kinematic coordinates of each of the three particles (momenta and production vertices); it is defined as the ratio between the number of events surviving the reconstruction, and the total number of generated events. It embeds the reconstruction efficiency as well as the geometric acceptance of the apparatus, while distortions due to inefficiencies of tracking detectors are not included. In the experimental plots shown in the following the bin errors account for the systematic uncertainty of the acceptance correction and the statistical uncertainty of the experimental bin, added in quadrature. A two-dimensional projection of the multidimensional acceptance map is shown in Fig. 2, integrated over the full target's fiducial volume, as a contour plot of the momentum of the $(\pi^- n)$ pair versus the proton momentum.

TABLE I. Average contaminations per event (over eight targets) of physical background reactions, for simulated events subject to the described analysis cuts and selected in the Σ^- invariant mass region. For the sake of comparison, the last line reports the reconstruction efficiency for the signal reaction $K^-_{\rm stop}(np)\ [A-np] \to \Sigma^- p\ [A-np]$.

Reaction	Contamination ($\times 10^{-7}$/event)
$K^-_{\rm stop} p\ [A-p] \to \Sigma^+ \pi^-\ [A-p]$	120.5 ± 3.3
$K^-_{\rm stop} np\ [A-np] \to \Sigma^0 n\ [A-np],\ \Sigma^0 n \to \Lambda n$	30.1 ± 1.3
$K^-_{\rm stop} p\ [A-p] \to \Sigma^- \pi^+\ [A-p],\ \pi^+ n \to \pi^0 p$	11.8 ± 1.0
$K^-_{\rm stop} np\ [A-np] \to \Sigma^+ \pi^- n\ [A-np]$	8.8 ± 0.7
$K^-_{\rm stop} np\ [A-np] \to \Sigma^0 n\ [A-np]$	6.7 ± 1.0
$K^-_{\rm stop} np\ [A-np] \to \Lambda \pi^0 n\ [A-np]$	4.8 ± 0.6
$K^-_{\rm stop} p\ [A-p] \to \Sigma^0 \pi^0\ [A-p]$	4.6 ± 0.5
$K^-_{\rm stop} np\ [A-np] \to \Lambda n\ [A-np]$	2.4 ± 0.3
$K^-_{\rm stop} nn\ [A-nn] \to \Sigma^- n\ [A-nn],\ \Sigma^- p \to \Lambda n$	2.3 ± 0.4
$K^-_{\rm stop} np\ [A-np] \to \Sigma^- p\ [A-np]$	9469.8 ± 30.0

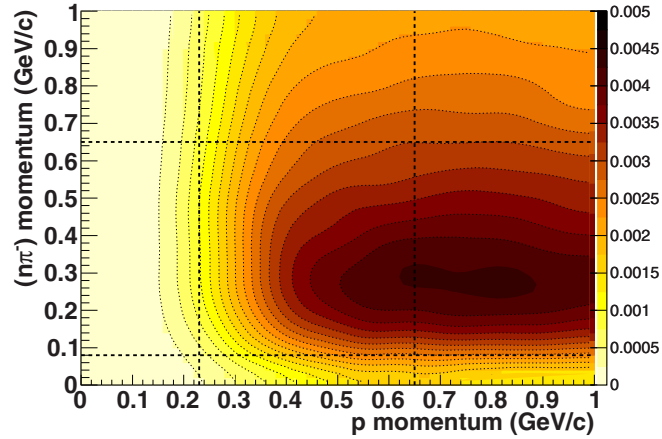

FIG. 2. (Color online) Two-dimensional projection of the acceptance multidimensional map for $n\pi^- p$ events emitted in K^- induced reactions, integrated over the full FINUDA target volumes.

The two-dimensional projection of the acceptance shows a moderate increase in the 200–500 MeV/c $(n\pi^-)$ pair momentum range. In the figure the dashed lines indicate the kinematic limits chosen for the analysis. Outside these limits the acceptance is small and its uncertainty large, consequently the correction would affect the experimental spectra with large systematic errors. The chosen ranges for the application of the acceptance correction are 80–650 MeV/c for the $(\pi^- n)$ pair, and 230–650 MeV/c for p. These ranges cover completely the $\Sigma^- p$ QF production kinematics.

IV. STUDY OF THE QF $K^- A \to \Sigma^- p\ [A-(np)]_{g.s.}$ REACTION

The invariant mass of the $(n\pi^-)$ pair for events selected in the B area of Fig. 1(a) is reported in the inset of Fig. 1(b). A similar fit with a Gaussian function and a fifth order Chebychev polynomial reports a large improvement of the S/B ratio, that becomes 2.38 for the ^{6}Li sample. Background subtracted data in the signal region F (evidenced in the picture in darker grey shade) are counted to evaluate the emission rates of the semi-inclusive QF $\Sigma^- p$ reaction.

Figure 3 reports, for the ^{6}Li targets, several acceptance corrected spectra obtained selecting events in a ± 6-MeV/c^2-wide window centered on the mean value of the Σ^- peak [E area in Fig. 1(b)]. The plots report, respectively, (a) the missing mass distribution, (b) the invariant mass of the $(n\pi^-)p$ system, (c) the distribution of the angle between the $(n\pi^-)$ system and

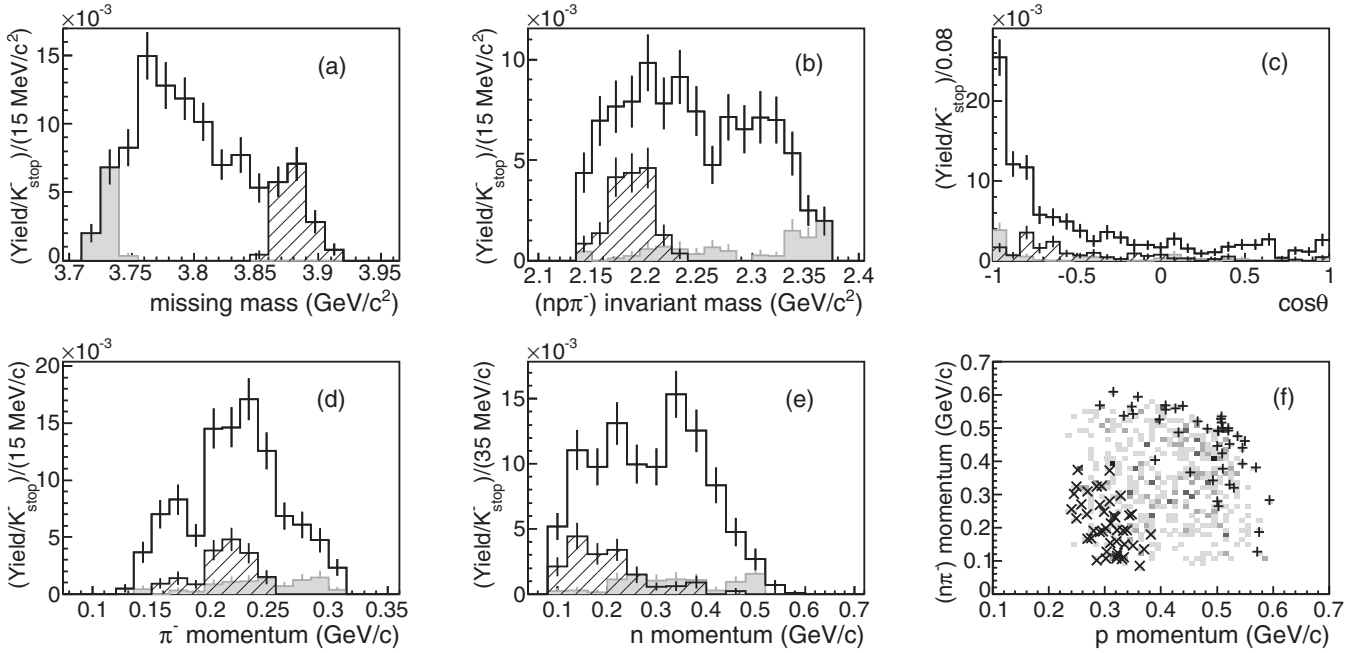

FIG. 3. Acceptance corrected distributions of some observables measured in the K^-_{stop} ^{6}Li $\rightarrow n\pi^- pA'$ reaction, with the invariant mass of the $(n\pi^-)$ pair selected in a 12-MeV/c^2 mass window centered on the Σ^- mass value. (a) Missing mass of the reaction, for events selected in the E region of the total missing mass plot of Fig. 1(b). The grey distribution corresponds to events belonging to region F only, the hatched one to events from region D of Fig. 1(a) after the selection in the Σ^- mass window (G). (b) Invariant mass distribution of the $(n\pi^-)p$ system, same selections. (c) Distribution of the angle between the $(n\pi^-)$ pair and the proton, same selections. (d), (e) Momentum distribution of the π^- and the neutron, same selections. (f) Scatter plot of the $(n\pi^-)$ system vs proton momentum. Events belonging to region F (upper right part, plus markers) and to the G sample (lower left part, cross markers) are superimposed.

the proton, the momenta distributions of (d) the π^- and (e) the neutron, and the scatter plot of the momentum of the $(n\pi^-)$ pair versus the proton momentum. The area of the plots is normalized to the total production rate of inclusive $\Sigma^- p$ final state described in the following section, which includes the background contribution.

In each (a)–(d) plot, the grey parts correspond to events selected in the F region of the $(n\pi^-)$ invariant mass plot shown in Fig. 1(b), while the hatched region corresponds to the subset of events located in the D region and selected in the mentioned Σ^- mass window (this data set will be called as G in the following as a shortcut).

In the missing mass spectrum of Fig. 3(a) the contributions from F and G samples are clearly seen. In the $(n\pi^-)p$ invariant mass distribution (b), the events from the semi-inclusive QF $\Sigma^- p$ reaction (F) tend to cluster in the region around 2.35 GeV/c^2. This corresponds to the threshold of the available phase space, while events compatible with an additional pion are located in a lower mass region. We recall that some of these events could also come from the $\Sigma^-\pi^0$ decay of $\Sigma^-(1385)$.

Figure 3(c) shows the distribution of the angle between the $(n\pi^-)$ pair and the proton. This distribution indicates that the events in the Σ^- band have a back-to-back correlation (grey histogram), as expected in a two-body quasifree absorption. On the other hand, the events selected in the hatched area (G) do not exhibit any favored topology, as typical of a three-body reaction.

Figures 3(d) and 3(e) report, respectively, the momentum distributions for the π^- and the neutron. No peculiar enhancement is observed in the distributions. The events selected in the Σ^- mass window distribute continuously in a similar way for both the decay particles (with a larger background contamination for neutrons), indicating that both are most likely coming from the decay in flight of the Σ^- [18].

Finally, in Fig. 3(f) the events from regions F and G are superimposed to the full scatter plot with different markers (pluses for F set, crosses for G set): the distribution in the upper right part of the pad corresponds to the events of set F, the one in the lower left corner to events of set G. Set F events prefer large momenta for both the $(n\pi^-)$ system and the proton, a typical feature of YN pairs produced in two-nucleon absorption, as mentioned earlier.

The acceptance corrected momentum distribution for prompt protons and for the $(n\pi^-)$ system selected in the Σ^- mass window for all the studied p-shell nuclei are shown in Fig. 4, normalized to the evaluated emission rates. In all of them, as in the previous pictures, the grey area corresponds to events selected in a missing mass window centered on the minimum recoiling mass nucleus (F), while the hatched areas to events located above the $\Sigma^- p\pi^0$ threshold (G). The proton momentum distributions indicate that most of the events in F area belong to semi-inclusive QF $\Sigma^- p$ reactions, and are characterized by momenta above 500 MeV/c. The same feature is shown by Σ^-'s, as already displayed in the scatter plot of Fig. 3(f) for ^{6}Li.

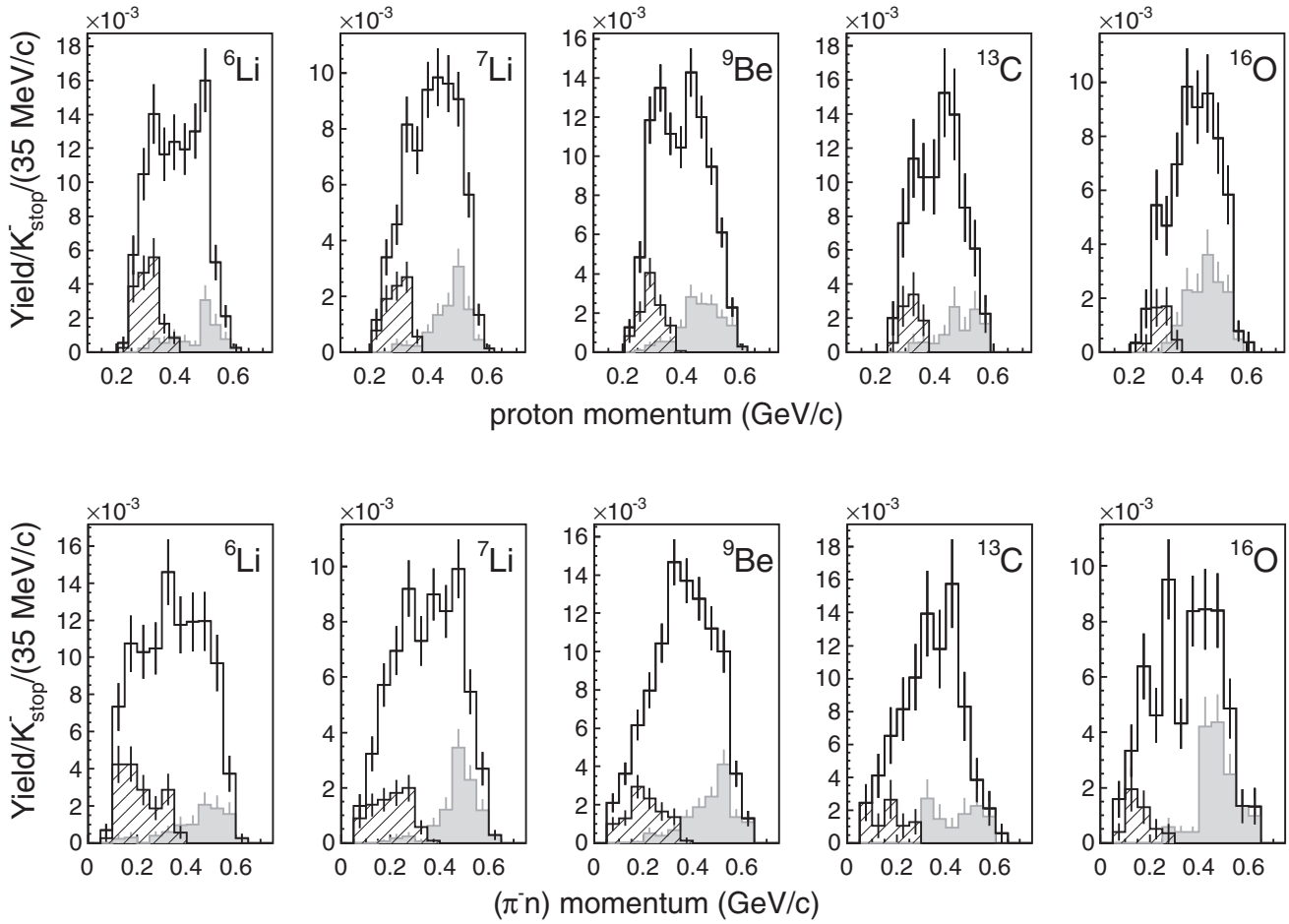

FIG. 4. Upper row: acceptance corrected proton momentum spectrum for all targets, for events selected in the E region of Fig. 1(b). The events in the grey area come from region F only, those in the hatched area from region G (see text for description). Lower row: selections as described above, $(n\pi^-)$ momentum distribution in the Σ^- mass region for all the targets.

A distinctive trait of the largest effect of FSI for heaviest nuclei can be seen in the broadening of the QF prompt proton signal as the target nucleus mass number increases, as already observed in Ref. [18].

V. EMISSION RATE EVALUATIONS

For reactions including Σ^-'s, emission rates only can be assessed, following the method already applied in several previous FINUDA papers [5,15,18]; in this analysis no correction is applied for possible pion attenuation effects nor for the Σ^- loss due to Σ-Λ undetected conversions. Following Ref. [15], the evaluated rates are finally scaled by the loss rate of slow Σ^-'s due to their single-nucleon capture in nuclei. Two data samples have been examined: events belonging to the full $(n\pi^-)$ invariant mass spectrum of Fig. 1(b) (region E), and events selected in the missing mass region corresponding to the semi-inclusive QF $\Sigma^- p$ reaction (inset, region F—we recall that by "semi-inclusive" the $\Sigma^- p$ production recoiling against a nuclear system in its minimum energy configuration is understood). The emission rate is defined, for each target, as

$$R_A = N_{\Sigma^- p}/N_{K^-_{\rm stop}}. \quad (2)$$

The numerator gives the absolute number of $\Sigma^- p$ events, which corresponds to the $N^C_{\Sigma^- p}$ events counted in the Σ^- peak of the $(n\pi^-)$ spectrum after proper background subtraction and corrected by the global efficiency of the channel: $N_{\Sigma^- p} = N^C_{\Sigma^- p}/\epsilon_{\Sigma^- p}$. The global efficiency can be factorized in two parts. The first depends on the trigger efficiency and reconstruction performance (determined, for each reaction, by the FINUDA Monte Carlo). The second one depends on the detectors' efficiencies, which are local and whose effects are different according to the event topology (track curvatures, charges, lengths, number of hits in each track, and number of tracks in a given apparatus sector). As far as the TOF and vertex detectors are concerned, their response was completely digitized in the FINUDA simulation code, where all thresholds and maps of inefficient channels had been listed: therefore, their instrumental inefficiency is taken into account at the hit definition and the following track reconstruction levels. Consequently, the efficiency for neutron detection is already embedded in the reconstruction. To get information on the detector efficiencies in the tracking volume $K_{\mu 2}$ decay real events have been used for positive tracks, while for negative tracks the information from Bhabha prongs as well as from the charged pions from K^0_S decays has been exploited. As figures

TABLE II. $\Sigma^- p$ emission rates in $K^-_{\rm stop}A$ absorption in several p-shell nuclei, listed in the first column. The second column, from Ref. [15], reports the correction factor for undetected Σ^-'s undergoing Σ-Λ conversion at rest. The third, fourth, fifth, and sixth columns report, respectively, the S/B ratio, the sensitivity $\mathscr{S}$, the number of observed $\Sigma^- p$ events after background subtraction, and the measured emission rate R_A, in units of $10^{-2}/K^-_{\rm stop}$. For each nuclear species, the first row refers to events belonging to the region marked as E in Fig. 1(b), the second one to events selected in the F region of Fig. 1(b). For all rates, statistical and systematic uncertainties are quoted. The systematic error has been evaluated adding in quadrature the contributions from the systematic uncertainty sources described in the text.

A	$\Sigma^-_{\rm loss}$ (10^{-2})	S/B	$\mathscr{S}$	$N^C_{\Sigma^- p}$	R_A $(10^{-2}/K^-_{\rm stop})$
^{6}Li	30 ± 2	0.84	15.48	828 ± 36	$4.72 \pm 0.61_{\rm stat} \pm 1.05_{\rm syst}$
		2.38	11.57	224 ± 18	$1.20 \pm 0.13_{\rm stat} \pm 0.27_{\rm syst}$
^{7}Li	26 ± 2	0.92	18.19	734 ± 42	$3.33 \pm 0.42_{\rm stat} \pm 0.52_{\rm syst}$
		2.56	11.95	211 ± 18	$0.67 \pm 0.08_{\rm stat} \pm 0.10_{\rm syst}$
^{9}Be	38 ± 2	0.92	17.22	983 ± 55	$4.67 \pm 0.59_{\rm stat} \pm 0.41_{\rm syst}$
		3.07	11.97	227 ± 17	$0.88 \pm 0.09_{\rm stat} \pm 0.03_{\rm syst}$
^{13}C	12 ± 1	0.90	11.43	395 ± 54	$4.15 \pm 0.78_{\rm stat} \pm 0.52_{\rm syst}$
		1.87	5.15	48 ± 9	$0.46 \pm 0.09_{\rm stat} \pm 0.02_{\rm syst}$
^{16}O	36 ± 3	1.21	12.36	348 ± 26	$3.42 \pm 0.65_{\rm stat} \pm 0.45_{\rm syst}$
		4.56	8.22	86 ± 17	$0.71 \pm 0.13_{\rm stat} \pm 0.05_{\rm syst}$

of merit, a typical integrated detector efficiency for a positive track of about 250 MeV/c is 73–78%, while for negative tracks of similar momentum it spans the range 63–86%. The inefficiencies are mainly due to the dead zones corresponding to aluminum supports, that were arranged to maximize the acceptance for ~270 MeV/c negative pions from hypernuclear decays. The difference among these efficiencies in different apparatus regions is also due to the performances of OSIM and LMDC's.

This part of the global efficiency carries the largest sources of systematic uncertainty in the evaluation of the emission rate, as will be reported in the following.

In the denominator of Eq. (2), the number of K^-'s stopped in each target is given by the reconstructed number of vertices, after the elimination of those with a fake $K^\pm$ assignment, scaled by the global $K^-_{\rm stop}$ detection efficiency: $N_{K^-_{\rm stop}} = N^{\rm Rec}_{K^-_{\rm stop}}/\epsilon_{K^-}$. This efficiency takes into account the trigger acceptance (depending on the reaction), and also the instrumental efficiency of the detectors delivering the trigger signal (TOFINO and TOFONE). Moreover, it includes the efficiency of the kaon stopping point determination procedure. ϵ_{K^-} can be evaluated, target by target, by a full simulation in which 14 types of QF reactions were injected (including rescattering and Σ-Λ conversion effects), each one with rates extrapolated from the few available measurements. The simulated statistics correspond to about 1.3 million $K^-_{\rm stop}$ events per target. The global $K^-_{\rm stop}$ detection efficiency varies in the range 22–46%, depending on the target; disfavored cases correspond to thicker targets (in particular, ^{13}C) for which the GEANE extrapolation is more critical.

This rate evaluation procedure, whenever possible, is tested against a second method based on the coincidence count of the searched topologies and the μ^+ from $K_{\mu 2}$ decay emitted from the opposite K^+ vertex, in the same ϕ decay (tagged events). Reactions with such a coincidence occur with a full trigger acceptance, but they suffer for reduced statistics and therefore they bear a larger statistical uncertainty. The two methods, when applied on samples of enough statistics (namely, on the inclusive sample E), lead to results in agreement within the statistical uncertainty. Their relative spread is taken into account as a source of systematic error.

Table II summarizes the results obtained for the rates evaluated for the E and F experimental subsets. They refer to the full kinematic range of the reactions. For each of the studied nuclei, the S/B value is reported (averaged, when two different targets of the same nuclear species are available) along with the sensitivity $\mathscr{S}$, which gives an estimation of the statistical significance of the observed signal. The subsequent columns report the number of counted $\Sigma^- p$ events, and the value of the emission rate, with both statistical and systematic errors. The total systematic error is obtained by summing in quadrature the contributions from different uncertainty sources, described in the following. When two targets are available, the weighted average of the rates obtained for each of them is reported. The spread between the values obtained for targets of the same species represents the second largest source of systematic error. This is especially true for the ^{6}Li targets whose geometrical position [in the $\phi(1020)$ antiboost direction] was unfavorable to stop kaons, a larger part of them being stopped by ISIM before they could reach the targets.

Table III reports the relative systematic errors for the two data samples, coming from different sources. Since the errors vary depending on the target composition and location, their maximum spread is quoted. In addition to the mentioned errors due to K^+/K^- identification inversion, different methods for the capture rate evaluation, target pairs located in different acceptance regions and tracking and detector efficiencies, other sources are due to changes in the selection criteria, to the peak/background fitting procedure, fitting functions and algorithm, and to the Σ^- window width chosen for the signal selection.

Overall, a maximum systematic error of 22% affects both the semi-inclusive and inclusive rates.

VI. DISCUSSION AND CONCLUSIONS

Figure 5 summarizes pictorially the available measurements of emission rates for the $K^-_{\rm stop}A \to \Sigma^- pA'$ reaction: the present measurements (Table II, full triangles

TABLE III. Relative systematic errors of $\Sigma^- p$ emission rates from different sources, for the semi-inclusive $K^-_{stop} A \to \Sigma^- p A'_{g.s.}$ reaction [$R(A'_{g.s.})$] and for the inclusive $K^-_{stop} A \to \Sigma^- p X A'$ one [$R(A')$]: the two values indicate the range of variability, depending on the target composition and location.

Syst. error source	$\Delta R(A'_{g.s.})/R(A'_{g.s.})$ (%)	$\Delta R(A')/R(A')$ (%)
K^+/K^- id. inversion and ISIM efficiency	0.4–1.9	0.4–1.9
μ tag rate evaluation		3–11
Tracking and tracking detector efficiencies	0.9–7.8	0.4–6.2
Targets in different acceptance regions	0–20	0–17
Selection and signal extraction efficiency	0.7–3.8	0.3–10.0
Total	4–22	9–22

and circles) add up to the few existing points on ^{4}He [1] (open triangle, open square, and open circle) and on ^{6}Li by the former FINUDA evaluations [18] (full square). For the measurements in ^{4}He, the open circle corresponds to $R(K^- {}^4\mathrm{He} \to \Sigma^- pd) = (1.6 \pm 0.6)\%/K^-_{stop}$, the open square to $R(K^- {}^4\mathrm{He} \to \Sigma^- ppn) = (2.0 \pm 0.7)\%/K^-_{stop}$, and the open triangle to the sum of $R(K^- {}^4\mathrm{He} \to \Sigma^- p\pi^0 np) = (1.0 \pm 0.4)\%/K^-_{stop}$, $R(K^- {}^4\mathrm{He} \to \Sigma^- p\pi^0 d) = (1.0 \pm 0.5)\%/K^-_{stop}$, and $R(K^- {}^4\mathrm{He} \to \Sigma^- p\pi^+ nn) = (1.4 \pm 0.5)\%/K^-_{stop}$. The former semi-inclusive FINUDA measurement on ^{6}Li was $R(K^- {}^6\mathrm{Li} \to \Sigma^- p[{}^6\mathrm{Li} - (np)]) = (1.62 \pm 0.75) \times 10^{-2}/K^-_{stop}$, where the statistical and systematic errors have been added in quadrature.

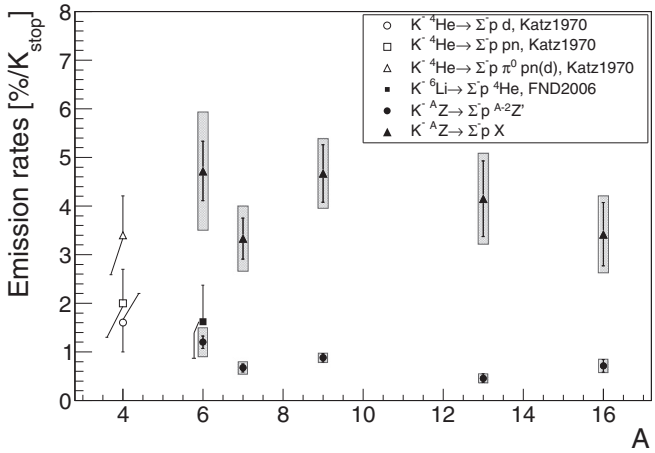

FIG. 5. Emission rates of the $K^- A \to \Sigma^- p[A - (np)]$ semi-inclusive and $K^- A \to \Sigma^- p X A'$ inclusive reactions for several nuclei. Measurements on ^{4}He are from [1], measurements for $A \geqslant 6$ are by FINUDA ([18] and present work). For the measurements described in the present paper, the error bars report the statistical uncertainty, while the grey boxes show the statistical and systematic error added in quadrature; for the other measurements, the total error is reported.

The full circles refer to the semi-inclusive QF $\Sigma^- p$ reaction (F set), while the full triangles are inclusive measurements from the E set. The error bars report the statistical uncertainty; the total error corresponds to the height of the shaded box (of arbitrary width). New and old measurements are in good agreement.

For inclusive measurements the systematic errors are large and any assessment about the existence of a trend as a function of the mass number is difficult; more interesting indications can be obtained by the more precise evaluation of the semi-inclusive QF $\Sigma^- p$ reaction. A remarkable decrease of the capture rate is evident for ^{7}Li as compared to ^{6}Li. This can be motivated by the presence of an additional neutron in ^{7}Li which enhances the probability of one-nucleon absorption as compared to the surface interaction of a K^- with a (np) pair. An analogous observation was made in the case of $\Sigma^\pm \pi^\mp$ productions [15], which both proceed via one-proton absorption of the kaon. The enhancement of the capture rate for ^{9}Be and ^{16}O can be accounted for considering the statistical increase of possible (np) absorption centers with the nucleus mass number. The average rates, over the $6 \leqslant A \leqslant 16$ mass number range, are $(0.69 \pm 0.05) \times 10^{-2}/K^-_{stop}$ for the semi-inclusive reactions, and $(3.94 \pm 0.36) \times 10^{-2}/K^-_{stop}$ for the inclusive ones, respectively. These new precision measurements can be fruitfully exploited, after proper extrapolations from the present ordinary temperature and density, as inputs to improve the current microscopic description of the hyperonic-nuclear matter EOS, crucial for a better understanding of dense astrophysical objects like compact stars [7]. These new data can also be useful to disclose the onset of excited baryonic states, like $\Lambda(1405)$ and $\Sigma(1385)$, in dense nuclear matter.

In conclusion, for the first time an assessment of the emission rates of the $K^- A \to \Sigma^- p A'$ reaction on some p-shell nuclei, with mass number in the range $6 \leqslant A \leqslant 16$, has been performed, complementing the quite few existing available measurements. It is shown that a sizable part of the experimental spectra fails to be explained by the simple QF two-nucleon $\Sigma^- p$ absorption reaction. Only an accurate spectral analysis would be able to disentangle the different contributions to the whole phase space volume, fully accounting for both contaminating reactions and other kaon induced reactions with $\Sigma^- p$ production [32]. $\Sigma^- p$ additional pairs can in fact be produced together with other undetected particles (pions and nucleons), and they may also come from the decay of more massive baryonic resonances.

Unfortunately, no experiment exists to date or is planned which will provide data of kaon induced reactions on the mentioned p-shell nuclei, comparable to the FINUDA data sample and to the same level of accuracy. The presented data are so far unique to get insight on the low energy kaon interactions in nuclei and, in general, in the strangeness nuclear physics scenario.

ACKNOWLEDGMENTS

The authors would like to thank A. Gal and J. Mareš for the careful reading of the manuscript and fruitful comments, suggestions, and discussions. This work was supported by INFN (Italy), by JSPS KAKENHI Grant No. 15340087 and by MEXT KAKENHI Grant No. 17070005 (Japan).

[1] P. A. Katz, K. Bunnell, M. Derrick, T. Fields, L. G. Hyman, and G. Keye, Phys. Rev. D **1**, 1267 (1970).

[2] T. Suzuki *et al.* (KEK-PS E549 Collaboration), Phys. Rev. C **76**, 068202 (2007).

[3] W. L. Knight, F. R. Stannard, F. Oppenheimer, B. Rickey, and R. Wilson, Nuovo Cimento **32**, 598 (1964); H. Davis, F. Oppenheimer, W. L. Knight, F. R. Stannard, and O. Treutler, Nuovo Cimento A **53**, 313 (1968).

[4] C. Vander Velde-Wilquet, J. Sacton, J. H. Wickens, D. N. Tovee, and D. H. Davis, Nuovo Cimento **39**, 538 (1977); J. W. Moulder, N. E. Garrett, L. M. Tucker, W. M. Bugg, G. T. Condo, H. O. Cohn, and R. D. McCulloch, Nucl. Phys. B **35**, 332 (1971).

[5] M. Agnello *et al.* (FINUDA Collaboration), Phys. Lett. B **698**, 219 (2011).

[6] M. Agnello *et al.* (FINUDA Collaboration), Nucl. Phys. A **835**, 439 (2010).

[7] D. Lonardoni, A. Lovato, S. Gandolfi, and F. Pederiva, Phys. Rev. Lett. **114**, 092301 (2015); D. Lonardoni, F. Pederiva, and S. Gandolfi, Phys. Rev. C **89**, 014314 (2014); D. Lonardoni, S. Gandolfi, and F. Pederiva, *ibid.* **87**, 041303(R) (2013); H.-J. Schulze and T. Rijken, *ibid.* **84**, 035801 (2011); I. Vidaña *et al.*, Europhys. Lett. **94**, 11002 (2011); I. Vidaña, I. Bombaci, A. Polls, and A. Ramos, Astron. Astrophys. **399**, 687 (2003).

[8] Y. Akaishi and T. Yamazaki, Phys. Rev. C **65**, 044005 (2002); T. Yamazaki and Y. Akaishi, Phys. Lett. B **535**, 70 (2002).

[9] M. Agnello *et al.*, Phys. Rev. Lett. **94**, 212303 (2005).

[10] G. Bendiscioli, T. Bressani, L. Lavezzi, and P. Salvini, Eur. Phys. J. A **40**, 11 (2009); G. Bendiscioli, T. Bressani, A. Fontana, L. Lavezzi, A. Panzarasa, and A. Rotondi, Nucl. Phys. A **789**, 222 (2007).

[11] T. Yamazaki *et al.* (DISTO Collaboration), Phys. Rev. Lett. **104**, 132502 (2010).

[12] K. Suzuki *et al.* (FOPI Collaboration), Prog. Theor. Phys. Suppl. **186**, 351 (2010).

[13] M. Agnello *et al.* (FINUDA Collaboration), Nucl. Phys. A **914**, 310 (2013).

[14] W. Weise and R. Härtle, Nucl. Phys. A **804**, 173 (2008); N. Shevchenko, A. Gal, and J. Mareš, Phys. Rev. Lett. **98**, 082301 (2007); A. Ramos and E. Oset, Nucl. Phys. A **671**, 481 (2000).

[15] M. Agnello *et al.* (FINUDA Collaboration), Phys. Lett. B **704**, 474 (2011).

[16] B. Loiseau and S. Wycech, Phys. Rev. C **63**, 034003 (2001); P. Heusi, H. P. Isaak, H. S. Pruys, R. Engfer, E. A. Hermes, T. Kozlowski, U. Sennhauser, and H. K. Walter, Nucl. Phys. A **407**, 429 (1983).

[17] E. J. Moniz, I. Sick, R. R. Whitney, J. R. Ficenec, R. D. Kephart, and W. P. Trower, Phys. Rev. Lett. **26**, 445 (1971).

[18] M. Agnello *et al.* (FINUDA Collaboration), Nucl. Phys. A **775**, 35 (2006).

[19] M. Agnello *et al.* (FINUDA Collaboration), Phys. Lett. B **622**, 35 (2005).

[20] J. Favier, T. Bressani, G. Charpak, L. Massonnet, W. E. Meyerhof, and Č. Zupančič, Nucl. Phys. A **169**, 540 (1971); C. Cernigoi, I. Gabrielli, N. Grion, G. Pauli, B. Saitta, R. A. Ricci, P. Boccaccio, and G. Viesti, *ibid.* **352**, 343 (1981); C. Cernigoi, N. Grion, G. Pauli, R. Rui, and R. Cherubini, *ibid.* **456**, 599 (1986).

[21] Y. Akaishi and T. Yamazaki, Nucl. Phys. A **792**, 229 (2007).

[22] V. Filippini, M. Marchesotti, and C. Marciano, Nucl. Instrum. Methods Phys. Res. A **424**, 343 (1999).

[23] P. Bottan *et al.*, Nucl. Instrum. Methods Phys. Res. A **427**, 423 (1999).

[24] M. Agnello *et al.*, Nucl. Instrum. Methods Phys. Res. A **385**, 58 (1997); M. Agnello *et al.*, *ibid.* **452**, 386 (2000).

[25] L. Benussi *et al.*, Nucl. Instrum. Methods Phys. Res. A **361**, 180 (1995); L. Benussi *et al.*, *ibid.* **419**, 648 (1998).

[26] M. Agnello *et al.* (FINUDA Collaboration), Phys. Lett. B **654**, 80 (2007).

[27] M. Agnello *et al.* (FINUDA Collaboration), Phys. Lett. B **669**, 229 (2008).

[28] A. Pantaleo *et al.*, Nucl. Instrum. Methods Phys. Res. A **545**, 593 (2005).

[29] B. Dalena, Ph.D. thesis, Università degli Studi di Bari, 2006 (http://inspirehep.net/record/712914/files/712914.pdf).

[30] V. Innocente, M. Maire, and E. Nagy, *GEANE: Average Tracking and Error Propagation Package CERN Program Library W5013-E*, 1991.

[31] M. Agnello *et al.* (FINUDA Collaboration), Phys. Lett. B **701**, 556 (2011).

[32] A. Filippi and S. Piano, Hyperfine Interactions **233**, 151 (2015).